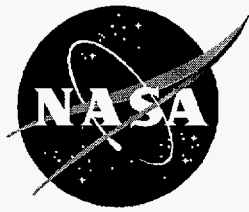


Electric Field Magnitude and Radar Reflectivity as a Function of Distance from Cloud Edge

Jennifer G. Ward and Francis J. Merceret
NASA/Kennedy Space Center, FL

September 2004



Electric Field Magnitude and Radar Reflectivity as a Function of Distance from Cloud Edge

Jennifer G. Ward and Francis J. Merceret
NASA/Kennedy Space Center, FL

**National Aeronautics and
Space Administration**

Kennedy Space Center

September 2004

Acknowledgments

The authors acknowledge the assistance of Jim Dye, Sharon Lewis, and Mike Dye of the National Center for Atmospheric Research for supplying the data used in this project. The authors also acknowledge with gratitude the careful review of an earlier draft of this paper by Winifred Lambert of the Applied Meteorology Unit.

Mention a proprietary product or service or of the producer thereof does not constitute an endorsement thereof by either the author, the National Aeronautics and Space Administration or the United States Government.

Available from:

NASA Center for AeroSpace Information
7121 Standard Drive
Hanover, MD 21076-1320

National Technical Information Service
5285 Port Royal Road
Springfield, VA 22161

ABSTRACT

The results from analyses of data collected during a field investigation of thunderstorm anvil and debris clouds are reported. Statistics describing the magnitude of the electric field are determined as a function of distance from cloud edge. Statistics describing radar reflectivity near cloud edge are also determined. Both statistical analyses use *in-situ* airborne field mill and cloud physics data coupled with ground-based radar measurements obtained in east-central Florida during the summer convective seasons of 2000 and 2001.

The results indicated that the average electric field magnitude outside of anvil and debris clouds was less than 3 kV/m. The average radar reflectivity at the cloud edge ranged between 0 and 5 dBZ.

Introduction

Beginning in 1999, the Kennedy Space Center (KSC) sponsored an Airborne Field Mill (ABFM) experiment in support of its Lightning Launch Commit Criteria (LLCC) project. The LLCC project is intended to improve the weather constraints (launch commit criteria) designed to protect space launch vehicles, including the Space Shuttle, from natural and triggered lightning. If these constraints are violated, launch must be delayed or scrubbed until the weather improves. In 1999, the instrumentation for the project was developed, installed and tested on the University of North Dakota Citation II research aircraft that was to be used for the field campaigns the following years. The first ABFM field campaign took place in June 2000 (Merceret and Christian, 2000). A second field campaign of this project was conducted in February 2001 and a third in May-June 2001 for a total of 30 flight days. This paper reports on results from the two summer season campaigns.

The goal of the LLCC project is learn enough about the behavior of electric charge in and near clouds to safely relax the current LLCC. Although the current constraints are safe, they have a false alarm rate (rule violated when it would actually be safe to fly) of more than 90 percent in some cases (Hugh Christian, NASA/Marshall Spaceflight Center, private communication). This is due primarily to our ignorance of how charge behaves in the atmosphere compounded by the need for large margins to ensure safety where there is no room for error. The LLCC project is directed at reducing the ignorance component of this situation so that less restrictive yet even safer rules may be developed.

The field campaigns use *in-situ* measurements of in-cloud electric fields from an instrumented aircraft coupled with simultaneous measurement of the cloud particle habit, size and concentration by the same aircraft. A key component of the experimental design is to couple ground-based weather radar measurements with the *in-situ* cloud physics and electric field measurements from the aircraft. The target clouds for the summer campaigns were thunderstorm anvil and debris clouds that had become passive charge carriers. Clouds that contained active charge sources as indicated by the presence of lightning were excluded from the study. Details are presented in Merceret and Christian (2000).

The LLCC are developed by a group of internationally recognized experts on natural and triggered lightning convened by the aerospace community under the administrative leadership of the KSC Weather Office. This group of experts, called the Lightning Advisory Panel (LAP), recommends LLCC to the launch community, which then reviews them through a series of formal processes and adopts those it deems appropriate. The latest LLCC recommendations from the LAP are found in Krider *et al.* (1999). Except for minor changes, these represent the current LLCC used operationally at NASA and Department of Defense launch facilities.

An initial analysis of ABFM data from anvil and debris clouds was completed and presented to the LAP in 2002 and additional analysis was presented in 2003. With the new information in-hand, the LAP provided the 45th Weather Squadron with minor safety-driven LLCC changes in 2003. Major LLCC revisions are now under consideration by the LAP that should both enhance safety and increase launch availability. These revisions use a radar-based parameter to determine when the electric field within the cloud is low enough to pose no significant threat of natural or triggered lightning.

Some of the LLCC prohibit flight in close proximity to clouds that could be electrified. Even though the launch vehicle is not inside the cloud, it could be close enough to encounter fields produced by electric charge within the cloud. A minimum "stand-off" distance is required in order to assure that the launch vehicle does not encounter dangerous electric fields in the vicinity of electrified clouds. The investigation reported here examined anvil and debris clouds to determine the potential to safely reduce the stand-off distances in the anvil and debris rules. These results were presented to the LAP on August 11, 2004.

The current attached anvil cloud rule is as follows: Do not launch if the flight path will carry the vehicle within 5 NM of the nontransparent parts of attached anvil clouds for the first 3 hours after the time of the last lightning discharge that occurs in the parent cloud or anvil cloud (Krider *et al.*, 1999, Rule 3a).

The current debris cloud rule (Krider *et al.*, 1999, Rule 4) is similar with a few extra constraints: Do not launch if the flight path will carry the vehicle within 5 NM of any nontransparent parts of a debris cloud during the 3-hour period after the last lightning occurrence in the cloud unless [all three of the following constraints are met],

1. There is at least one working field mill within 5 NM of the debris cloud
2. The absolute values of all electric field measurements at the surface within 5 NM of the flight path and at the mill(s) specified in (1) above have been less than 1000 V/m for 15 minutes
3. The maximum radar return from any part of the debris cloud within 5 NM of the flight path has been less than 10 dBZ for 15 minutes (*ibid*).

Both of these rules require a stand-off distance of 5 NM. If this could safely be reduced, it would result in fewer scrubbed launches since these rules would be violated less frequently. For example, if the stand-off distance were reduced to 3 NM, then those violations of the current rule where the flight path is between 3 and 5 miles from the cloud edge would not be violations of the revised rule.

1. Project Plan

In this project we analyzed the magnitude of the electric field decay as a function of distance from cloud edge using ABFM data and an automated cloud edge detection algorithm. Similarly, we analyzed the radar reflectivity at the cloud boundary. The data were filtered to match the cloud types and altitudes being used to develop the new radar-based anvil and debris Lightning Launch Commit Criteria. The goal was to provide guidance to the LAP for possible modification of the LLCC stand-off distances. The radar-based LLCC currently being developed by the LAP will improve the parts of the rules relating to flight through cloud, while any changes resulting from this work will improve the parts of the rules relating to flight in clear air in the immediate vicinity of cloud. The electric field portion of this work relates directly to the stand-off distances discussed above. The radar portion relates to determining the location of the cloud edge by radar when no visual observation of the cloud is possible.

2. Instrumentation

In order to determine the magnitude of the electric field as a function of distance from the edge of a cloud, we needed to measure the electric field as a function of position and we needed to know the location of the cloud boundaries. The electric field was measured using "electric field mills" aboard the research aircraft as described below. The cloud boundaries were located using cloud physics measurements from the same aircraft as well as ground-based radar measurements as input to the automated cloud-edge detection algorithm developed by Ward and Merceret (2004).

Electric field mills use a spinning rotor similar in shape to a cloverleaf, (hence the name "mill") to alternately expose a set of stationery electrodes to and shield them from the ambient electric field. The resulting alternating current in the electrodes is proportional in amplitude to the normal component of the imposed vector field. Its phase determines the sign of the field. A minimum of four such mills appropriately located on an aircraft is necessary to resolve the three components of the ambient field through which the aircraft is flying. The fourth mill is required in order to allow calculation of the local field produced by any electric charge on the aircraft. For our field program, we used six mills. This provided a degree of redundancy and allowed for consistency checks that facilitated data quality control and accurate calibration of the system (Winn, 1993).

Two ground-based weather radars supported the program. The WSR-74C weather radar located at Patrick Air Force Base (PAFB) is a C-band (5.3 cm) weather radar that provides only reflectivity (precipitation) measurements. "WSR" in the name of the radar is a standard designation for "Weather Surveillance Radar". The PAFB radar is subject to significant attenuation in heavy rain. The WSR-88D weather radar located at the National Weather Service Office in Melbourne (MLB), FL is an S-band (10 cm) weather radar that has both Doppler (velocity) and reflectivity (precipitation) capability. Although attenuation does exist in heavy rain, it is rarely significant (Merceret and Ward, 2002). We only used the reflectivity measurements from the MLB radar.

The research aircraft was a Cessna Citation II owned and operated by the University of North Dakota (UND). The cloud microphysics instrumentation flown on the aircraft included the PMS Forward Scattering Spectrometer Probe (FSSP) that analyzed the cloud droplet spectrum, the PMS Optical Array 1D-C and 2D-C and the SPEC Cloud Particle Imager that measured cloud particle sizes, the SPEC High Volume Particle Sampler (HVPS) that measured precipitation particles, the PMS King Probe that measured the liquid water content, and the Rosemount Icing Rate Meter that measured the super-cooled liquid water content. For a detailed description of these instruments and the performance characteristics of the aircraft see Ward *et al.* (2003).

3. Data Collection, Selection and Primary Quality Control

The data for this study were taken from ABFM data files created and maintained by the National Center for Atmospheric Research (NCAR) under the direction of Drs. Jim Dye and Sharon Lewis with assistance from other NCAR personnel and the ABFM science team under contract to NASA. These data were carefully calibrated and extensively quality controlled by members of the science team, and data from different sources were carefully time synchronized. The synchronized data from the various sources were combined into single "merged" files for each flight day. The merged files included radar reflectivity from the PAFB and MLB radars, cloud

physics and electric field measurements from the UND Citation, and the full suite of Citation navigation and air data measurements.

We used only those flights or portions of flights in which the clouds had been flagged as anvil clouds or debris clouds. Any data taken in a radar scan gap or radar void were rejected. This insured that the automated cloud-edge detection algorithm (see section 5) had access to the required radar data. For a discussion of the gaps and voids in the PAFB and MLB radar scan strategies, see Short (2000) and Taylor (1994). In addition, data at an altitude lower than 5000 feet were also rejected. Below this altitude the temperature could be warm enough that mixed phase (ice and water both present) was possible. The concept of anvil adopted for this study required that no charge generators be present, and charge generation is possible when mixed phases are present.

4. The Automated Ingest and Secondary QC Process

The merged files are extremely large and contain many variables that are not necessary for this study. In addition, every record needed to be checked to determine whether it satisfies the “filter” conditions for cloud type, altitude and radar availability. In order to produce smaller files containing only the data necessary for this analysis, Merceret wrote a program in Microsoft Visual Basic® to ingest the merged files and reformat them into working files with the unnecessary variables eliminated. This program also performed additional automated quality control and flagged every record not meeting the desired selection criteria. It identified every cloud entry or exit and wrote the electric field and radar reflectivity values for 100 seconds of flight on either side of the cloud boundary to a separate log file in a fixed column-width text format.

5. Automated Cloud Edge Detection Algorithm

In order to determine the behavior of the electric field and radar reflectivity with respect to the distance from the cloud boundary, we needed to know the location of the clouds and their boundaries. This information was available in the merged files either explicitly or implicitly. Cloud entry and exit times were determined based on *in-situ* cloud physics and ground based weather radar measurements from the merged files using the algorithm described by Ward and Merceret (2004).

The details of the algorithm are available in the literature (*ibid*), but the essence requires two steps. First, determine the presence of cloud at each point along the flight path from the cloud physics data, with an assist from the ground-based radar under certain conditions. Second, at each point along the flight track where the in-cloud status changes from true to false or false to true, perform a hysteresis check. The hysteresis check requires that the in-cloud status not change for at least 2 km on each side of the current change of status. This eliminates fuzzy, ill-defined cloud boundaries or false cloud boundary indications due to instrument noise.

6. Microsoft Excel® Analysis

The electric field and reflectivity log files generated by the Visual Basic program were imported to Microsoft Excel® where the data could be analyzed graphically and statistically. The following procedure was applied to separate anvil and debris cloud workbooks. First, each flight’s cloud entry and exit logs were imported from the workbooks generated for the individual

flights into corresponding individual worksheets in a master workbook. These sheets were then copied onto a single master sheet in that workbook. Each record on the master sheet contained the Flight ID, the word “entry” or “exit”, the UTC of exit or entry, and the electric field or radar reflectivity for 100 seconds before and after the exit or entry in ten second intervals.

The electric field values were denoted by $E(n)$ and the reflectivity values by $R(n)$ where n is an integer index ranging from -10 to 10. The index is equal to zero for the record at which the change of cloud state occurs. It is equal to 1 for the next record after the change of state and two for the next and so on. It equals -1 for the record immediately preceding the change of state, -2 for the one before that and so on. Since records were produced every ten seconds, and the aircraft flew at approximately 100 m/s, the index roughly corresponds to the distance in kilometers from the cloud boundary. For flight legs entering a cloud, positive indices were in cloud. For legs exiting a cloud, positive indices were out of cloud. Before the statistics were computed, the spreadsheet entries for exit and entry legs were aligned so that all data in a single column represented the same distance in the same direction from the cloud boundary.

The records were sorted by the value of the radar reflectivity or electric field at the cloud boundary to identify duplicate records. The ABFM data set included files which differed only by the grid coordinates assigned to the aircraft position for purposes of plotting the data on the ABFM website. This multiple gridding allowed graphical renditions in which the aircraft stayed on the grid, but it meant that more than one file contained the same data. When sorted, identical records were easy to identify and remove to avoid biasing the analysis. A record was defined as a duplicate only if the time and all 21 $R(n)$ or $E(n)$ values were identical.

Ideally, we would like to know the precise distance from cloud edge to the location of each measurement. Although in principle this can be determined from the data in the merged files plus the ABFM radar archive CAPPI plots, the labor required would be prohibitive. As an alternative we used the speed of the aircraft and the time between records to estimate the distance. As noted above, the aircraft flew at an approximate speed of 100 m/s. Thus, the ten seconds between records corresponded to about 1 km of horizontal distance. For this reason we have interpreted the index, n , in the $R(n)$ in each record to be the distance in km from the cloud edge. This required us to delete some otherwise valid entry and exit records as described next.

7. Manual QC Process to Delete Unsuitable Records

The ABFM website contains graphical presentations of the microphysics, electric field and radar data. These are called “MER” plots because of the kinds of data they contain. The cloud physics and reflectivity profiles from each record’s MER plot were examined manually to determine if the clear air portion of the flight track was “clean” or contaminated. A contaminated entry or exit is defined as one in which the clear air portion of the record remained close to overhanging or underlying cloud although the time from the cloud boundary would suggest a much larger distance. These contaminated cases had to be deleted because the indicated distance from the cloud was substantially greater than the actual distance. This would make the statistics relating electric field or reflectivity to distance meaningless. An example of a contaminated entry is presented in Figure 1. The aircraft was flying less than 1 km below cloud base for nearly 50 seconds (5 km of horizontal distance) before cloud entry at 18:35:50 UTC. Thus fields that would be identified as being from 1 to 5 km from the cloud edge are actually fields from less than 1 km below cloud.

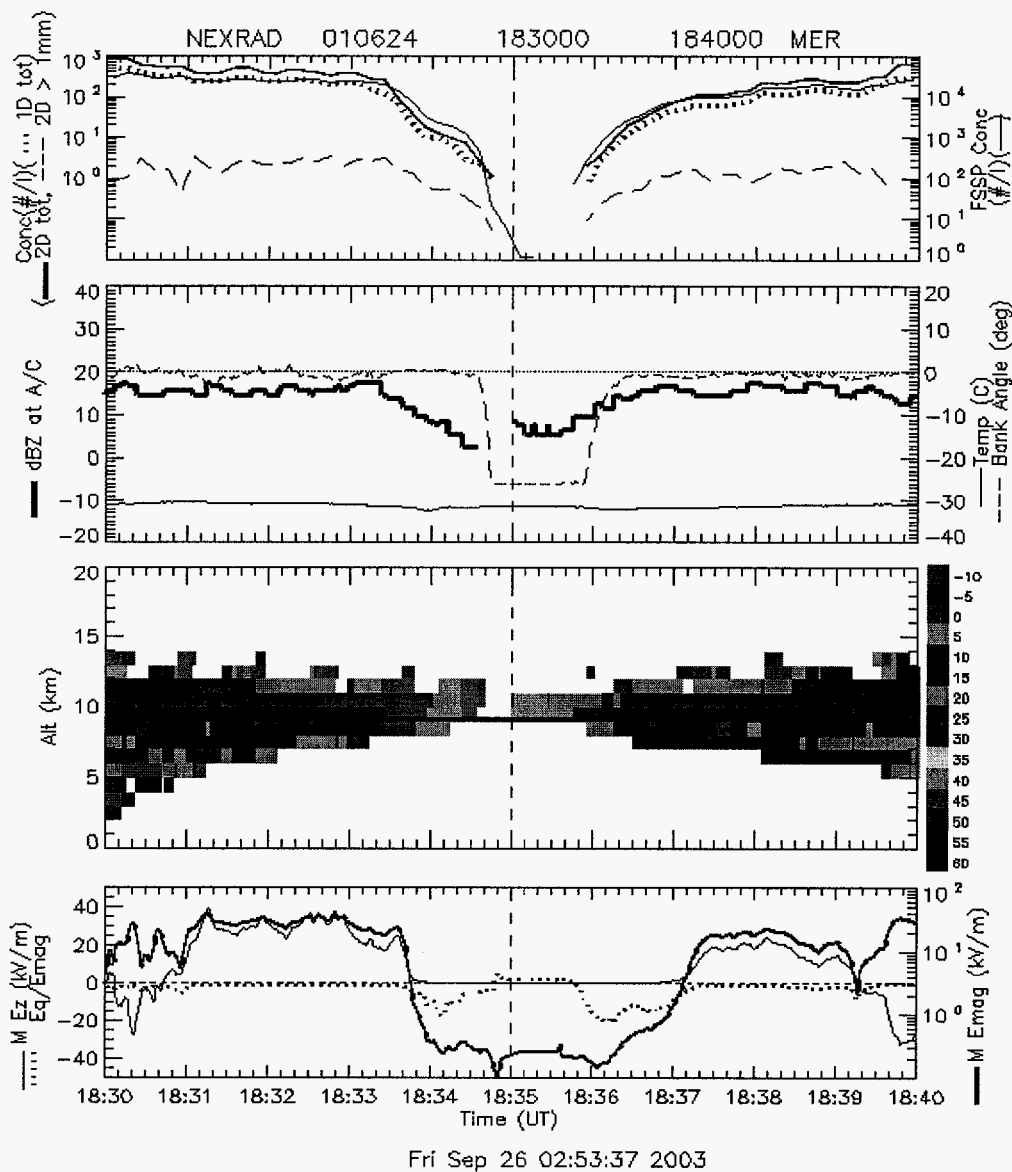


Figure 1. Microphysics, electric field and radar (MER) plot for 24 June 2001, 18:30 to 18:40 UTC. Radar data are from the Melbourne WSR-88D (NEXRAD) radar. The top panel shows the microphysics measurements. The second panel shows the air temperature, aircraft bank angle, and the radar reflectivity at the aircraft position. These are also not of concern here, nor is the bottom panel which shows the electric field measured by the aircraft. The third panel presents a vertical cross section of the radar reflectivity along the aircraft flight track. The value of the reflectivity in dBZ is color coded. The vertical axis is altitude in km and the horizontal axis is time (UTC). The aircraft position is given by the solid black line near 9 km altitude. The aircraft entered the cloud at 18:35:50, but was flying less than 1 km below cloud base beginning at 18:35:00.

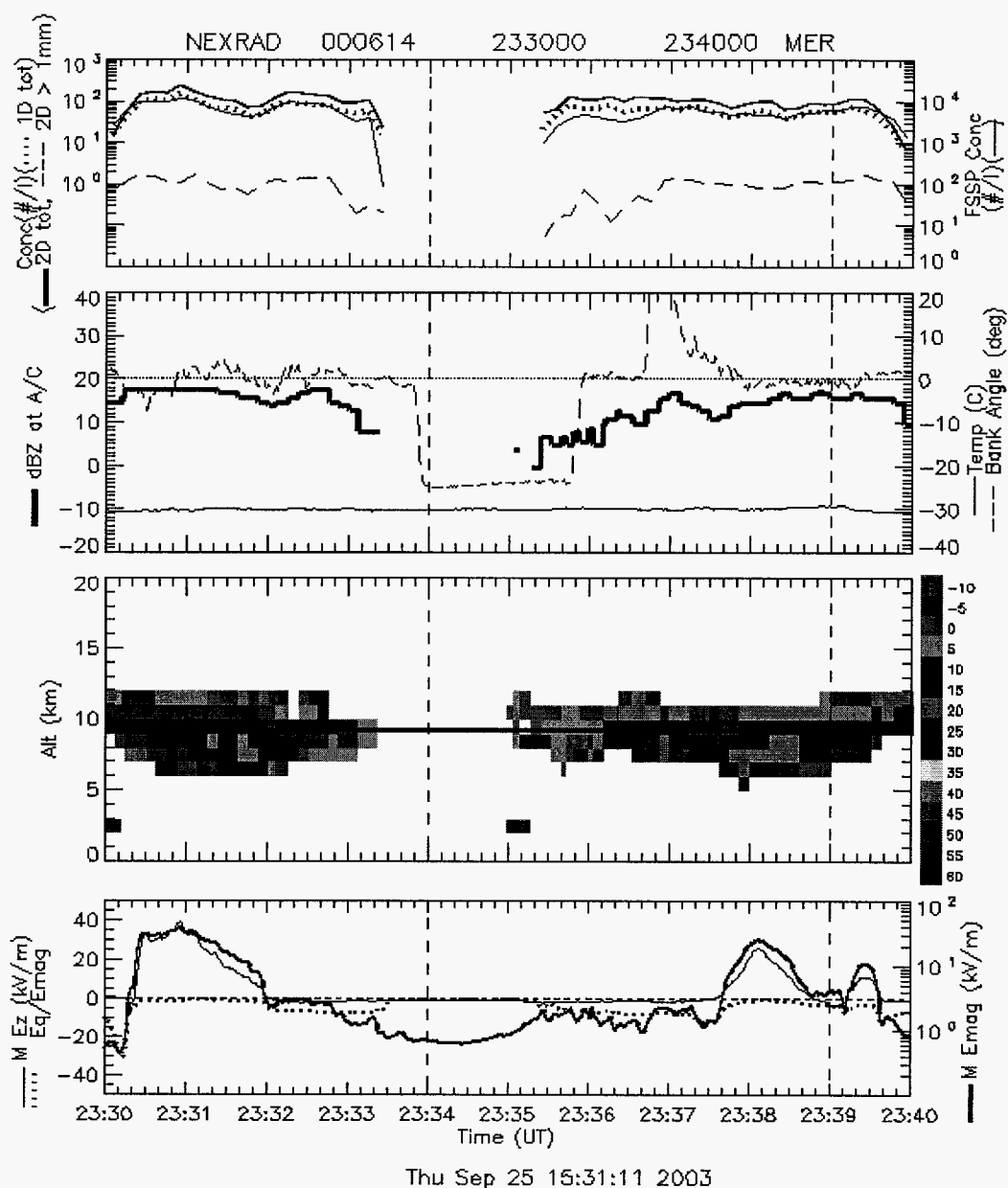


Figure 2. Microphysics, electric field and radar (MER) plot for 14 June 2000, 23:30 to 23:40 UTC. Radar data are from the Melbourne WSR-88D (NEXRAD) radar. The aircraft exited the cloud at 23:33:20 and re-entered cloud at 23:35:00.

Figure 2 presents a clean exit followed by a clean entrance. The aircraft exited the cloud at 23:33:20 and re-entered cloud at 23:35:00. Here there is no overhanging or under hanging cloud, and the distance from cloud boundary estimated from the time and aircraft speed corresponds to the actual distance from the cloud.

8. Electric Field Results

We computed statistics for anvil and debris cloud separately in case they had different characteristics. For each value of n , the minimum, mean, median, maximum, standard deviation, skewness coefficient and kurtosis coefficient were computed over all $E(n)$ in the data. The most useful results are those for the maximum and the mean. The median values tracked the mean values rather closely although they tended to be systematically a bit smaller. The complete statistical tables for anvil and debris clouds with maximum electric fields $\geq 3\text{ kV/m}$ are presented in Appendix I, Tables 1 and 2 respectively.

Figure 3 presents the minimum, average and maximum magnitude of the electric field as a function of distance from anvil edges for anvils with maximum electric field magnitude $\geq 3\text{ kV/m}$. This threshold was selected after discussions with the Lightning Advisory Panel, who determined that fields $< 3\text{ kV/m}$ do not pose a threat to launch vehicles. Including these non-threatening cases in the statistics would bias the averages to the low side, thus potentially masking the true extent of large fields outside of clouds that are hazardous. Entry and exit data are plotted separately along with the values obtained by combining them.

Well inside the cloud (distances from -5 to -10 km) the electric fields are quite large. The maxima exceed 10 kV/m and the averages exceed the danger threshold of 3 kV/m . Closer to the cloud edge, the field strength decreases. The maximum fields drop below 3 kV/m inside the cloud before the edge is reached, and the average field magnitude is below 1 kV/m at cloud edge and outside the cloud.

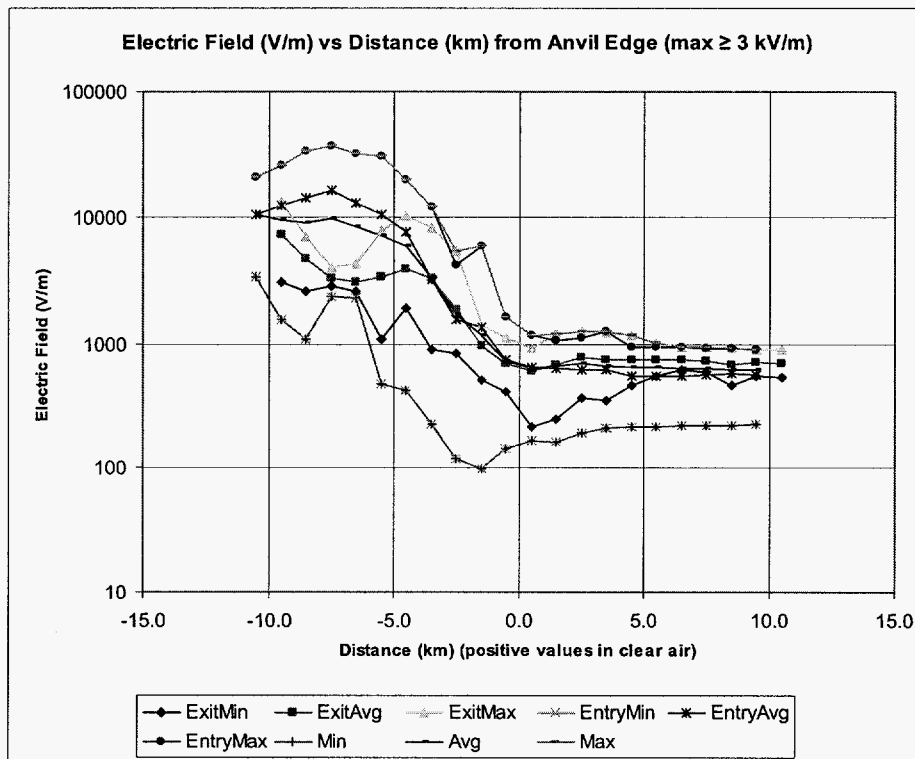


Figure 3. The magnitude of the electric field as a function of distance from the edge of anvil clouds with electric fields $\geq 3\text{ kV/m}$. Positive distance values are outside of cloud, negative values within. Minimum, average and maximum values are shown for flight legs entering clouds (entry), leaving clouds (exit) and both combined.

Figure 4 shows the same information for clouds with maximum fields of 1 kV/m or more. Figure 5 shows the same information when all data are included. These 2 analyses were done to see what effect they would have in the results compared to using only data with electric fields ≥ 3 kV/m. The maximum curves did not change because the maxima were all contained in the ≥ 3 kV/m data. The conclusions don't change significantly although the average and minimum curves in Figures 4 and 5 drop off faster and to a lower value than those in Figure 3 as expected.

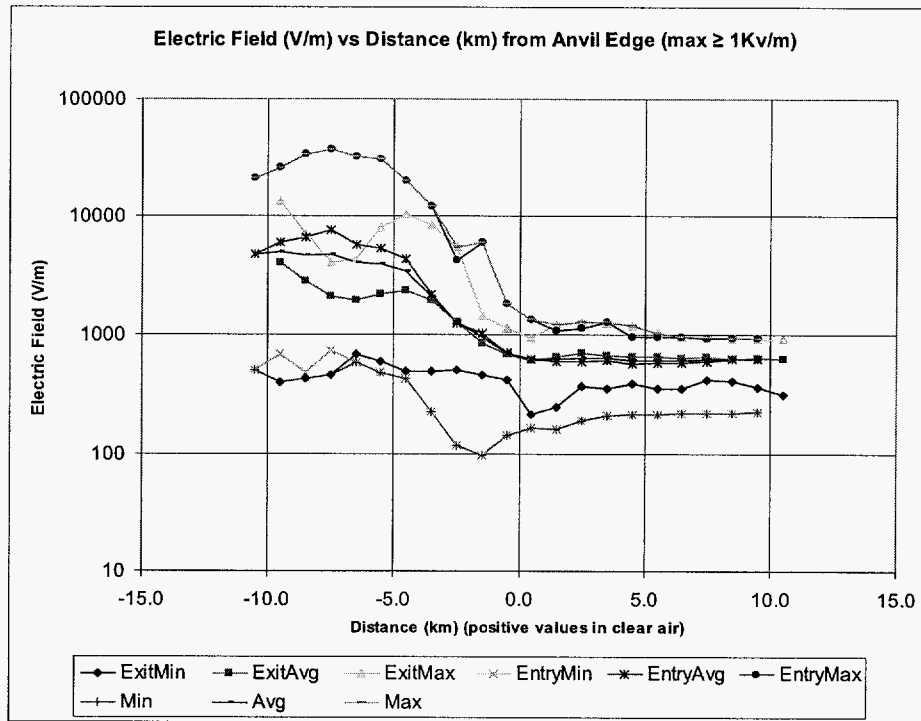


Figure 4. Same as Figure 3 except data from cases with maxima between 1 and 3 kV/m are included.

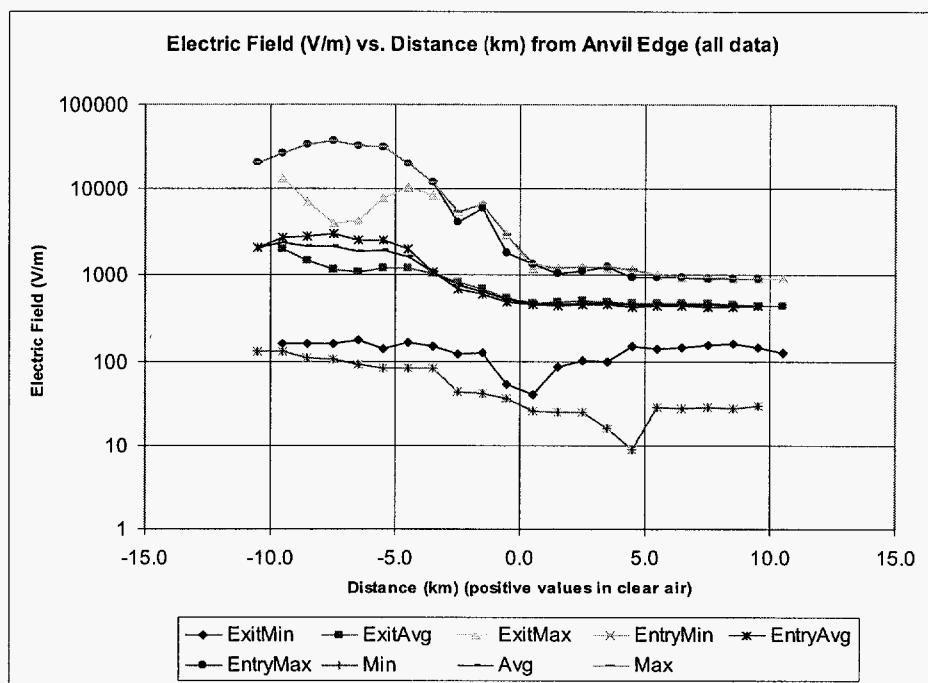


Figure 5. Same as Figure 3 except all data are included.

Figures 6, 7 and 8 present the same data for debris cloud as Figures 3, 4 and 5 respectively present for anvils. The results are similar.

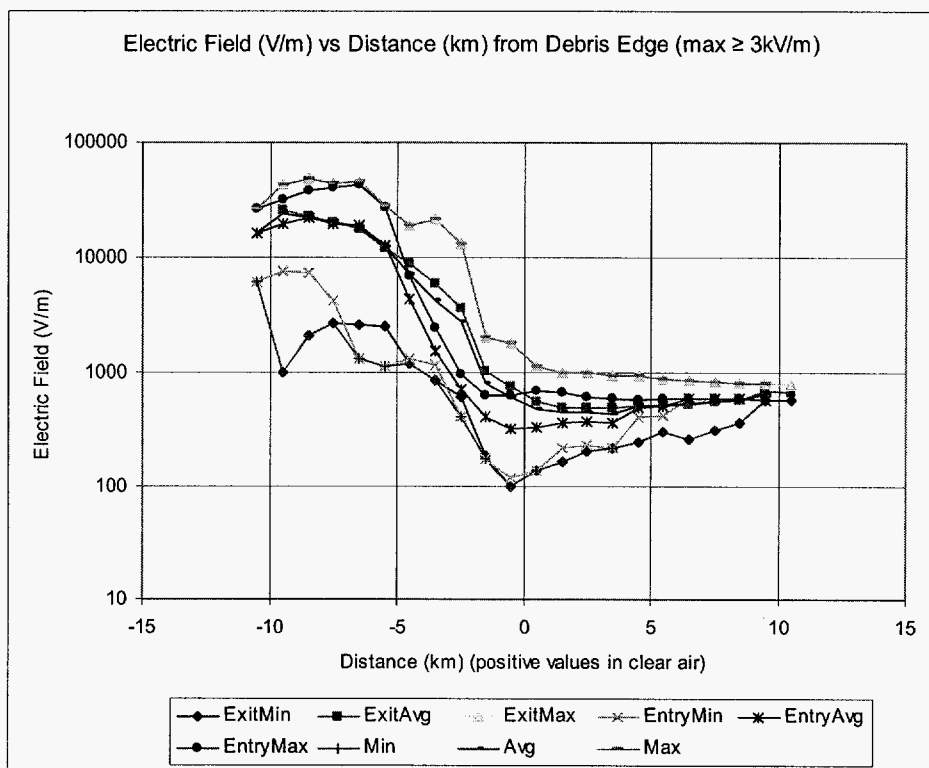


Figure 6. Same presentation as Figure 3 except for debris cloud rather than anvil cloud.

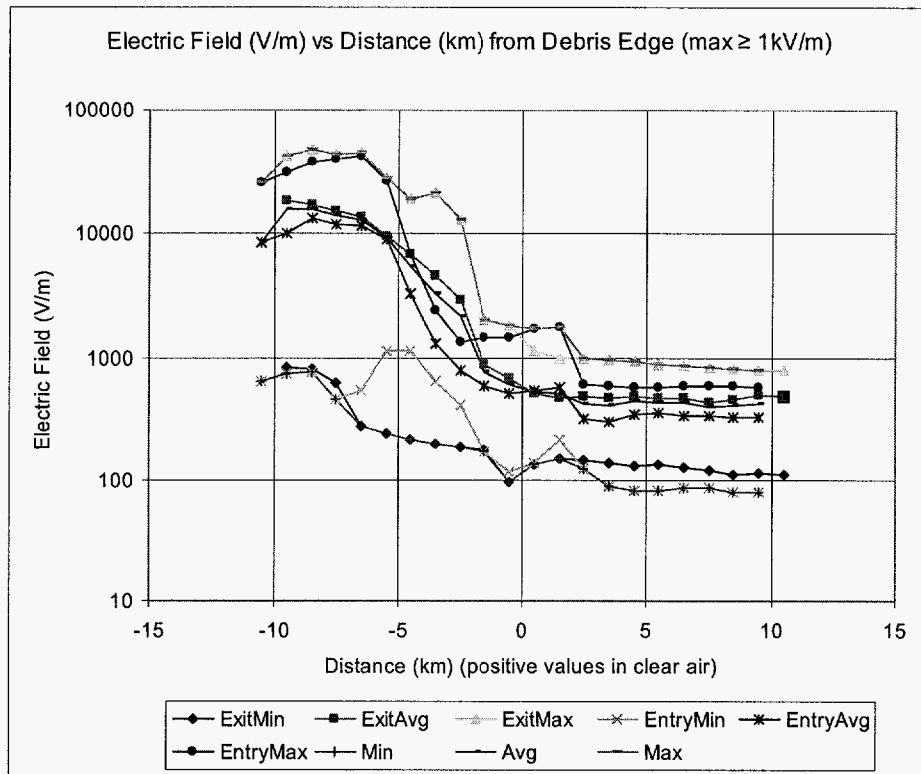


Figure 7. Same presentation as Figure 4 except for debris cloud rather than anvil cloud.

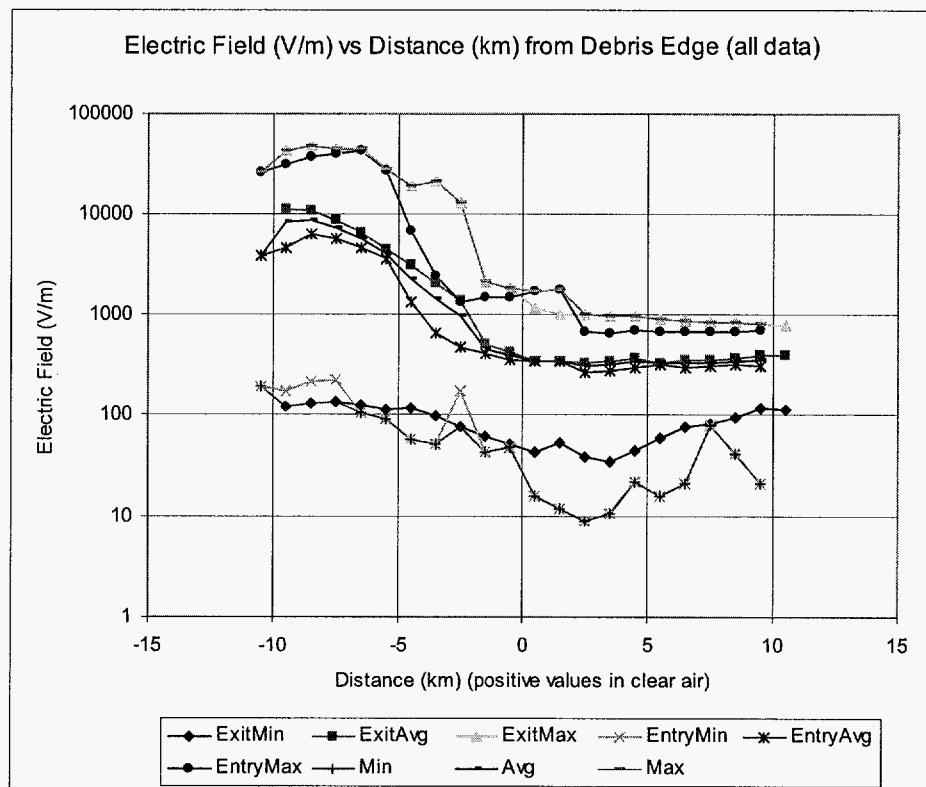


Figure 8. Same presentation as Figure 5 except for debris cloud rather than anvil cloud.

9. Electric Field Comparison to ABFM I

In the early 1990's Marshall Spaceflight Center conducted an airborne field mill program similar to that described here, but without the extensive cloud physics instrumentation or WSR-88D data (Christian *et al.*, 1993). They performed a similar analysis of the decay of the electric field magnitude with distance from cloud edge, but for convective clouds associated with active thunderstorm cores rather than the passive anvils or debris clouds studied here.

Although the target environments are very different, we are including a comparison of the results from the two programs, denoting the earlier program as ABFM-I and the current program as ABFM-II. The results for the average and maximum values are presented in Figure 9. For the ABFM-II data, the anvil and debris data were combined in the following fashion: The maximum electric field plotted is the largest of the anvil or debris maximum at each distance. The plotted average is the largest of the anvil or debris average at each distance. Thus both the average and the maximum for ABFM-II are the larger (most hazardous) of the anvil or debris data.

The ABFM-I data show much larger fields at each distance. In private conversation with Dr. Douglas Mach of the University of Alabama-Huntsville, the supplier of the ABFM-I data, we concluded that this is almost certainly due to the very different environments in which the data were taken. The ABFM-II results presented above are valid for anvils and debris clouds without active charge sources. The ABFM-I data were taken in active convective clouds, many of which were producing lightning.

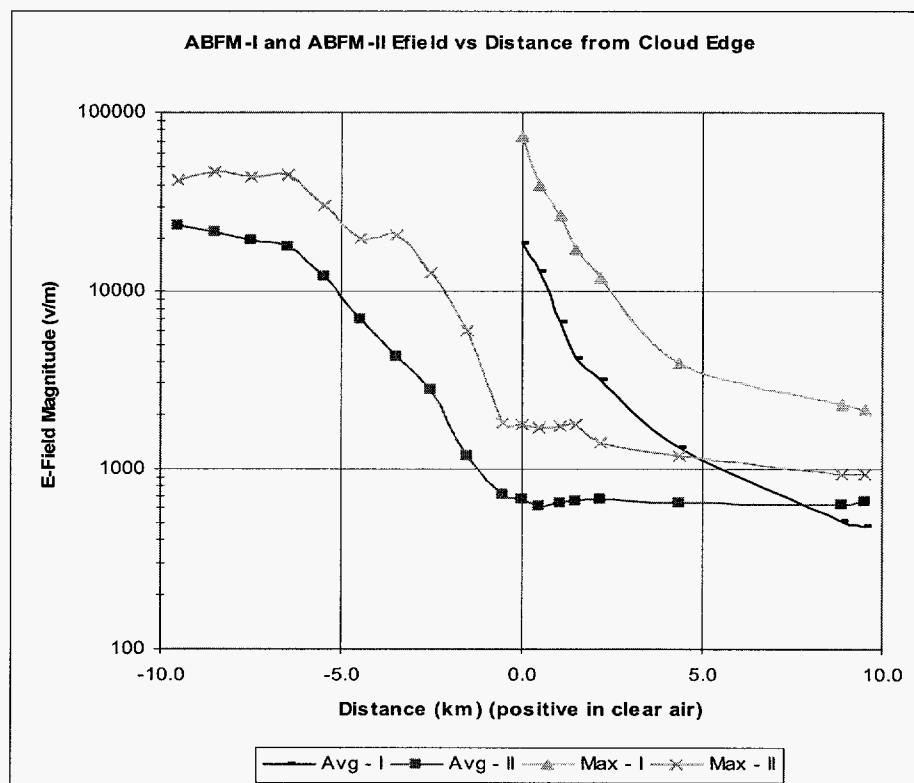


Figure 9. Maximum and average electric field as a function of distance from the edge of clouds for ABFM-I and ABFM-II. The ABFM-I data were not available inside the cloud so those curves are present only for positive distance values.

10. Reflectivity Results

As for the electric field, we computed radar statistics for anvil and debris cloud separately in case they had different characteristics. For the same reason, we computed separate statistics for the WSR-74C and the WSR-88D. For each value of n , the minimum, mean, median, maximum, standard deviation, skewness coefficient and kurtosis coefficient were computed over all $R(n)$ in the data. Again, the most useful results are those for the maximum and the average. The median values tracked the mean values rather closely although they tended to be systematically a bit smaller. The complete statistical tables for anvil and debris clouds are presented in Appendix I, Tables 3 and 4 respectively.

Figure 10 presents the minimum, average and maximum magnitude of the reflectivity as a function of distance from anvil edges for both radars. The minimum reflectivity is really a measure of the minimum detectable signal of the radar and the amount of ground clutter, anomalous propagation and clear air reflectivity present in the data. The maximum and average reflectivities are larger within the cloud than in clear air as expected with a transition region across the cloud boundary. The average data from the two radars agree within the error of measurement (± 1 dB for each radar).

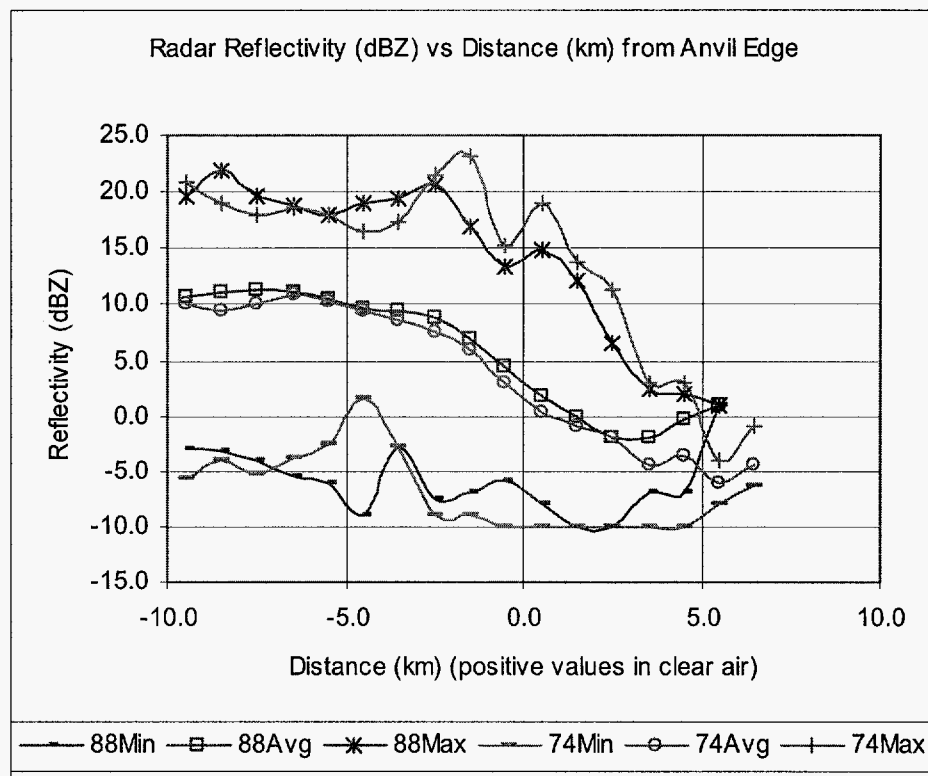


Figure 10. Maximum, average and minimum reflectivity (dBZ) as a function of distance from cloud edge for the PAFB ("74") and MLB ("88") radars. Positive distances are outside of cloud, negative distances are in cloud.

Figure 11 shows the same information for debris clouds. In this case the average value for the WSR-74C is lower than that for the WSR-88D by slightly more than the error of measurement. This may be due to the low reflectivity cutoff imposed on the WSR-88D by the National Weather Service to preserve adequate signal to noise ratio for some of their algorithms (Fang and Doviak, 2001). The cut-off can bias the average WSR-88D reflectivity to the high side.

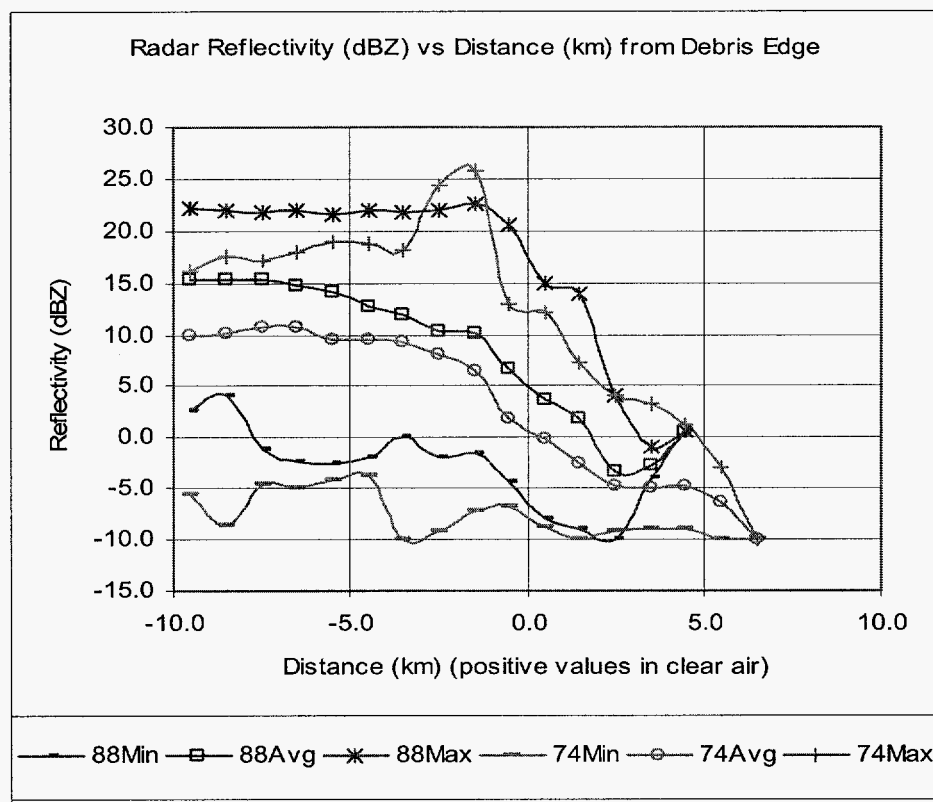


Figure 11. Same presentation as Figure 10 except for debris clouds.

In both cases, the average reflectivity at the cloud boundary is between 0 and 5 dBZ. This is consistent with the current LLCC definition of the radar cloud boundary as 0 dBZ. The definition is close to but just below the measured average value. This makes it safe, but not unnecessarily restrictive.

11. Reflectivity vs. Electric Field Comparison

One goal of the current series of field campaigns was to determine if radar reflectivity could be used to diagnose the presence or absence of hazardous in-cloud fields. The ABFM science team produced scatter diagrams of electric field magnitude vs. reflectivity on a point by point basis. These scatter diagrams showed that low reflectivity implied low fields and high fields implied high reflectivity, but the linear correlation was poor. Figure 12 presents an example. We thought it would be informative to plot the average electric field obtained from our analysis as a function of the average radar reflectivity from our analysis at the same distance. This would hide much of the detail but the averaging would reduce the scatter. The result is shown on Figure 13.

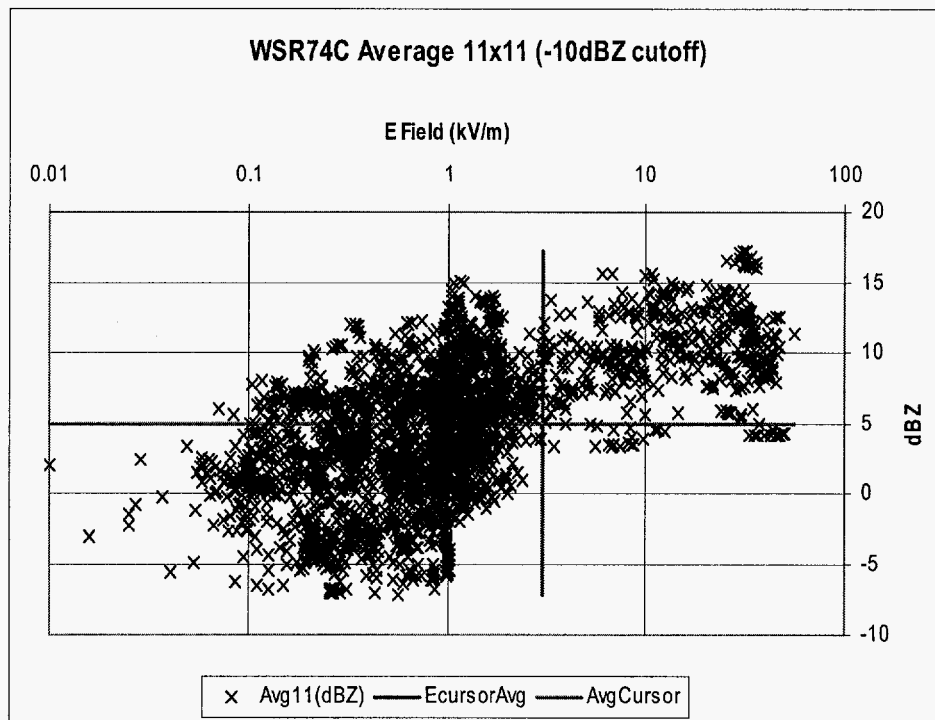


Figure 12. Typical ABFM scatter plot of radar reflectivity averaged over all clouds above 5 km altitude in a moving 11x11 km (horizontal) box centered on the aircraft position as a function of electric field magnitude. Each point represents a single 10-second record using PAFB radar data. All applicable anvil data are included in this one plot.

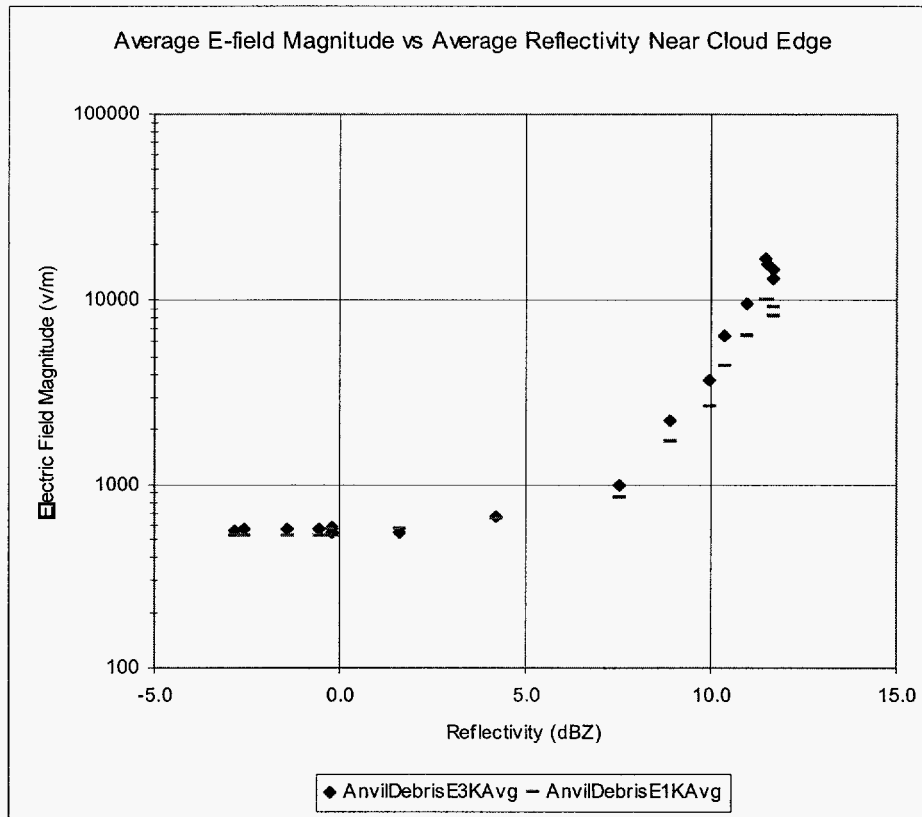


Figure 13. Average electric field magnitude as a function of average radar reflectivity at the same distance from cloud edge derived from the results presented in this paper. The distance from cloud edge is a hidden parameter that does not appear explicitly in the graph, but the larger fields and reflectivities correspond to more negative (in-cloud) values of the distance.

The remarkable thing about Figure 13 is the high correlation and minimal scatter. For the region with fields above 1 kV/m, the data can be fit by an exponential function with $r^2 = 0.97$. For reflectivities below 5 dBZ it is clear that the data rapidly approach an asymptotic value between 500 and 600 V/m. This is consistent with ABFM teleconference discussions that below a reflectivity of about 5 dBZ, a cloud without generators can no longer store charge for a significant period of time.

12. Conclusions

There are six major findings from this work.

- Anvil and debris clouds behave similarly and a single model can be used for both.
- Electric fields outside of anvil and debris clouds did not exceed 3 kV/m.
- Fields outside of convective clouds with active charge generators were larger than those of anvil or debris clouds at distances less than 5 - 10 km.
- The WSR-74C average reflectivity at cloud edge was slightly lower than that of the WSR-88D.
- Reflectivity measured by either radar at cloud edge for both anvil and debris clouds fell between 0 and 5 dBZ, consistent with the current LLCC definition.
- Average electric fields and average radar reflectivities in the vicinity of cloud boundaries were highly correlated in a manner consistent with previous ABFM discussions and analyses.

These results have several consequences for revision of the LLCC. First, they support the validity of the current radar definition of cloud edge in the LLCC. Second, they support the validity of the analysis by the ABFM science team relating hazardous fields to reflectivities above 5 dBZ. That analysis is the basis for revisions to the anvil and debris rules currently being drafted by the LAP. Finally, the rapid decay of the electric field with distance from cloud edge suggests the possibility for additional LLCC revisions reducing the stand-off distances in one or more of the rules. This could safely provide additional launch availability.

References

- Christian, H.J., D.M. Mach and J.C. Bailey, 1993: The Airborne Field Mill Project: A Program Summary, A32E-03, EOS Transactions, Vol. 74, No. 43, October 26, 1993, Supplement.
- Fang, Ming and Richard J. Doviak, 2001: Spectrum Width Statistics of Various Weather Phenomena, "Remote Sensing of Turbulence: RADAR Activities", FY01 Year-End Report, Appendix A, NCAR/RAP, 55pp. [Available on the WWW at http://www.rap.ucar.edu/projects/faa_turb/fy01_year_end_report_App_A.pdf.]
- Krider, E.P., H.C. Koons, R.L. Walterscheid, W.D. Rust, and J.C. Willett, 1999: Natural and Triggered Lightning Launch Commit Criteria (LCC), Aerospace Report No. TR-99(1413)-1, The Aerospace Co., El Segundo, CA, 15pp.
- Merceret, F.J. and H. Christian, 2000: KSC ABFM 2000 - A Field Program to Facilitate Safe Relaxation of the Lightning Launch Commit Criteria for the American Space Program, Paper 6.4, 9th AMS Conference on Aviation and Range Meteorology, Orlando, Florida, 11-15 September 2000.
- Merceret, Francis J. and Jennifer G. Ward, 2002: Attenuation of Weather Radar Signals Due to Wetting of the Radome by Rainwater or Incomplete Filling of the Beam Volume, NASA Technical Memorandum TM-2002-211171, April 2002, 16pp.
- Short, David, 2000: Final Report on IRIS Product Recommendations, NASA Contractor Report Number 2000-208572, ENSCO, Inc., Cocoa Beach, FL, 18pp.
- Taylor, Gregory E., 1994: Report on the Comparison of the Scan Strategies Employed by the Patrick Air Force Base WSR-74C/McGill Radar and the NWS Melbourne WSR-88D Radar, NASA Contractor Report Number 196291, ENSCO, Inc., Cocoa Beach, FL, July 1994, 32pp.
- Ward, Jennifer G., and Francis J. Merceret, 2004: An Automated Cloud-Edge Detection Algorithm Using Cloud Physics and Radar Data. *J. Atmos. Oceanic Technol.*, **21**, 762 – 765.
- Ward, Jennifer G., F.J. Merceret, and C.A. Grainger, 2003: An Automated Cloud-edge Detection Algorithm Using Cloud Physics and Radar Data, NASA Technical Memorandum TM-2003-211189, June 2003, 14pp.
- Winn, W. P., 1993: Aircraft measurement of electric field: Self-calibration, *J. Geophys. Res.*, **98**, 6351-6365.

Appendices

Appendix I - Electric Field Statistical Tables

Exit																						
Distance (km)	-10.5	-9.5	-8.5	-7.5	-6.5	-5.5	-4.5	-3.5	-2.5	-1.5	-0.5	0.5	1.5	2.5	3.5	4.5	5.5	6.5	7.5	8.5	9.5	10.5
Count		6	6	5	5	7	7	7	7	8	8	8	8	7	6	6	6	5	5	5	3	3
Minimum		3074	2616	2888	2620	1093	1925	909	837	515	409	212	246	363	347	462	546	612	586	467	547	539
Mean		7359	4736	3268	3098	3400	3927	3299	1883	968	690	602	683	783	737	752	741	747	723	675	714	696
Median		7570	4884	2942	2758	2809	2672	1856	1333	995	605	545	673	731	722	703	687	702	688	676	694	659
Maximum		13364	7030	3977	4248	7968	10360	8401	5411	1418	1123	926	1191	1245	1222	1164	1004	946	948	919	901	891
Std. Dev.		3779	1735	503	673	2235	3063	2916	1575	277	268	263	308	278	288	256	197	147	152	174	178	179
Skewness		0.50	-0.04	0.87	1.80	1.67	2.00	1.31	2.50	-0.14	0.64	-0.03	0.16	0.32	0.65	0.77	0.59	0.59	0.84	0.35	0.50	0.90
Kurtosis		3.07	1.44	1.20	6.15	6.37	6.92	3.01	9.46	3.36	1.82	1.59	2.69	3.78	4.77	3.03	1.20	1.02	2.52	2.64		
Entry																						
Distance (km)	-10.5	-9.5	-8.5	-7.5	-6.5	-5.5	-4.5	-3.5	-2.5	-1.5	-0.5	0.5	1.5	2.5	3.5	4.5	5.5	6.5	7.5	8.5	9.5	
Count	4	5	5	5	6	8	9	9	9	10	10	10	10	9	9	7	7	7	6	5	5	
Minimum	3348	1542	1088	2370	2306	478	425	225	116	98	143	162	158	190	205	212	212	219	219	219	223	
Mean	10496	12307	14258	16519	13176	10501	7662	3259	1535	1332	748	643	631	614	617	550	551	550	565	568	562	
Median	8834.5	7387	2757	6351	6456	3646	2964	1415	1071	912	622.5	495	536.5	543	545	557	574	579	562	568	527	
Maximum	20967	26013	33703	36930	32016	30847	20205	12083	4159	6024	1639	1160	1064	1118	1255	946	940	934	922	910	903	
Std. Dev.	8338	11981	16633	16610	13949	11631	8336	3918	1319	1711	445	332	298	287	319	242	239	236	253	282	283	
Skewness	0.65	0.47	0.61	0.62	0.81	1.03	0.77	1.70	1.12	2.75	0.91	0.46	0.07	0.53	0.98	0.32	0.29	0.33	0.06	-0.03	0.09	
Kurtosis	0.70	-0.11	-0.25	-0.01	1.11	2.38	1.41	5.67	3.65	11.11	3.53	2.03	1.76	2.89	3.88	3.00	3.04	2.98	2.41	1.25	1.00	
Combined																						
Distance (km)	-10.5	-9.5	-8.5	-7.5	-6.5	-5.5	-4.5	-3.5	-2.5	-1.5	-0.5	0.5	1.5	2.5	3.5	4.5	5.5	6.5	7.5	8.5	9.5	
Total Count	4	11	11	10	11	15	16	16	16	18	18	18	18	16	15	13	13	12	11	10	8	
Grand Min	3348	1542	1088	2370	2306	478	425	225	116	98	143	162	158	190	205	212	212	219	219	219	223	
Grand Average	10496	9608	9064	9894	8595	7187	6028	3277	1688	1170	722	625	654	688	665	643	639	632	637	622	619	
Grand Max	20967	26013	33703	36930	32016	30847	20205	12083	5411	6024	1639	1160	1191	1245	1255	1164	1004	946	948	919	903	

Table 1. Statistics for the electric field in anvil clouds for those records where the maximum electric field magnitude is not less than 3 kV/m. The kurtosis coefficient is defined such that it equals 3.0 for a Gaussian distribution, the standard statistical definition, rather than the Microsoft Excel® definition that subtracts 3 from the standard quantity to make a Gaussian kurtosis equal to zero.

Exit																						
Distance (km)	-10.5	-9.5	-8.5	-7.5	-6.5	-5.5	-4.5	-3.5	-2.5	-1.5	-0.5	0.5	1.5	2.5	3.5	4.5	5.5	6.5	7.5	8.5	9.5	10.5
Count		5	6	6	6	7	7	7	7	7	7	7	7	6	6	6	3	3	3	3	2	2
Minimum		1008	2101	2672	2605	2490	1192	851	610	187	99	137	164	205	217	249	302	260	312	361	582	584
Mean		25405	22155	19776	17625	11851	8611	5776	3653	1024	767	564	495	503	496	508	524	526	554	577	691	683
Median		31849	21047	17000	11710	8754	6604	2344	1304	707	768	604	391	299	300	360	396	465	526	558	691	683
Maximum		42272	47477	43793	44862	27812	18802	20947	12829	2043	1806	1126	987	995	955	935	873	853	824	811	800	781
Std. Dev.		16866	19815	18091	16725	9068	7141	7180	4544	678	545	316	299	365	348	308	306	301	257	226	154	139
Skewness		-0.79	0.17	0.27	0.96	0.90	0.86	2.04	1.77	0.46	1.10	0.66	0.98	0.93	0.93	0.89	1.55	0.87	0.48	0.37		
Kurtosis		2.12	0.45	0.53	2.68	3.11	1.92	7.13	5.69	1.72	4.94	4.00	2.62	1.18	1.14	1.25						
Entry																						
Distance (km)	-10.5	-9.5	-8.5	-7.5	-6.5	-5.5	-4.5	-3.5	-2.5	-1.5	-0.5	0.5	1.5	2.5	3.5	4.5	5.5	6.5	7.5	8.5	9.5	10.5
Count	2	2	3	3	3	4	4	4	3	4	4	4	4	4	4	2	2	1	1	1	1	
Minimum	6049	7380	7308	4197	1327	1126	1308	1170	417	174	118	139	219	231	217	407	426	598	590	590	584	
Mean	15956	19362	21462	19239	18423	12731	4362	1527	718	419	320	333	369	371	363	493	507	598	590	590	584	
Median	15956	19362	19603	13622	11659	11631	4681	1255	782	431	265	249	296	317	320	493	507	598	590	590	584	
Maximum	25862	31344	37476	39897	42284	26538	6778	2429	956	641	633	694	663	621	596	579	588	598	590	590	584	
Std. Dev.	14010	16945	15170	18501	21300	11457	2500	603	275	196	223	249	204	175	170	122	115					
Skewness			0.54	1.24	1.28	0.38	-0.47	1.97	-0.99	-0.32	1.30	1.62	1.60	1.47	1.16							
Kurtosis						0.55	0.50	6.90		3.30	4.91	5.66	5.44	5.01	3.66							
Combined																						
Distance (km)	-10.5	-9.5	-8.5	-7.5	-6.5	-5.5	-4.5	-3.5	-2.5	-1.5	-0.5	0.5	1.5	2.5	3.5	4.5	5.5	6.5	7.5	8.5	9.5	10.5
Total Count	2	7	9	9	9	11	11	11	10	11	11	11	11	10	10	8	5	4	4	4	3	
Grand Min	6049	1008	2101	2672	1327	1126	1192	851	417	174	99	137	164	205	217	249	302	260	312	361	582	
Grand Average	15956	23678	21924	19597	17891	12171	7066	4231	2773	804	605	480	449	451	443	504	517	544	563	580	655	
Grand Max	25862	42272	47477	43793	44862	27812	18802	20947	12829	2043	1806	1126	987	995	955	935	873	853	824	811	800	

Table 2. The same as Table 1 except for debris cloud.

Appendix II - Radar Statistical Tables

88Exit	-9.50	-8.50	-7.50	-6.50	-5.50	-4.50	-3.50	-2.50	-1.50	-0.50	0.50	1.50	2.50	3.50	4.50	5.50	6.50
Count	10	11	12	12	16	16	17	19	19	21	21	13	11	9	6	2	1
Minimum	0.30	-1.20	1.00	0.00	-1.30	-2.40	-2.00	-2.90	-4.00	-5.80	-7.00	-8.40	-10.00	-7.00	-7.00	1.00	5.40
Mean	12.09	12.15	13.02	12.24	11.35	10.99	9.76	9.38	7.52	4.57	2.07	-0.93	-2.21	-1.44	0.83	4.70	5.40
Median	13.65	13.60	14.00	13.60	11.95	11.10	10.20	10.30	7.80	4.00	1.80	-2.90	-3.00	-2.20	1.50	4.70	5.40
Maximum	17.40	16.40	19.40	18.00	17.40	17.30	16.00	16.40	17.00	12.80	12.00	12.10	6.60	7.40	8.00	8.40	5.40
Std. Dev.	5.47	5.13	4.65	4.74	4.74	4.68	5.21	4.84	5.31	4.79	5.29	5.46	5.19	4.50	4.88	5.23	
Skewness	-1.26	-1.98	-1.61	-1.78	-1.30	-1.46	-1.24	-0.99	-0.32	-0.16	0.02	1.21	0.39	0.80	-0.30		
Kurtosis	4.10	7.49	6.80	6.71	5.45	6.78	4.29	4.22	3.05	3.10	2.23	4.55	2.48	3.56	4.70		
88Entry	-9.50	-8.50	-7.50	-6.50	-5.50	-4.50	-3.50	-2.50	-1.50	-0.50	0.50	1.50	2.50	3.50	4.50	5.50	6.50
Count	14	15	16	22	23	24	23	24	25	26	26	13	4	4	1	2	0
Minimum	-3.00	-3.20	-4.00	-5.40	-6.00	-9.00	-2.80	-7.60	-7.00	-5.00	-8.00	-10.00	-4.00	-3.50	1.00	1.00	
Mean	9.79	10.37	10.14	10.58	9.92	8.70	9.27	8.33	6.81	4.51	1.87	1.02	0.63	-0.73	1.00	1.50	
Median	11.40	10.30	10.15	10.70	11.20	10.90	10.00	9.20	6.00	3.25	1.55	1.00	1.40	0.00	1.00	1.50	
Maximum	19.60	21.80	19.70	18.80	18.00	19.00	19.40	20.60	16.10	13.40	14.80	9.20	3.70	0.60	1.00	2.00	
Std. Dev.	6.29	6.39	6.00	5.73	5.73	6.99	6.09	6.49	5.68	5.05	6.08	4.69	3.41	1.88		0.71	
Skewness	-0.45	-0.15	-0.55	-0.99	-0.97	-0.82	-0.46	-0.63	-0.43	0.34	0.29	-0.60	-1.04	-1.82			
Kurtosis	2.87	3.41	3.70	4.49	4.12	3.33	2.38	3.57	3.38	2.39	2.66	4.99	3.33	6.41			
88All	-9.50	-8.50	-7.50	-6.50	-5.50	-4.50	-3.50	-2.50	-1.50	-0.50	0.50	1.50	2.50	3.50	4.50	5.50	6.50
Total Count	24	26	28	34	39	40	40	43	44	47	47	26	15	13	7	4	1
Grand Min	-3.00	-3.20	-4.00	-5.40	-6.00	-9.00	-2.80	-7.60	-7.00	-5.80	-8.00	-10.00	-10.00	-7.00	-7.00	1.00	5.40
Grand Average	10.75	11.12	11.37	11.16	10.51	9.62	9.48	8.80	7.12	4.54	1.96	0.04	-1.45	-1.22	0.86	3.10	5.40
Grand Max	19.60	21.80	19.70	18.80	18.00	19.00	19.40	20.60	17.00	13.40	14.80	12.10	6.60	7.40	8.00	8.40	5.40

Table 3a. Same as Table 1 except the data are radar reflectivity for WSR-88D.

74Exit	-9.50	-8.50	-7.50	-6.50	-5.50	-4.50	-3.50	-2.50	-1.50	-0.50	0.50	1.50	2.50	3.50	4.50	5.50	6.50
Count	22.00	26.00	27.00	27.00	30.00	31.00	33.00	39.00	41.00	42.00	42.00	31.00	23.00	12.00	9.00	3.00	2.00
Minimum	-5.60	-2.80	-5.30	-3.90	-2.60	1.50	0.90	-1.90	-3.80	-7.80	-9.00	-10.00	-10.00	-10.00	-10.00	-8.00	-6.30
Mean	9.89	9.20	9.42	9.82	8.99	8.98	8.67	7.61	6.16	3.31	-0.04	-1.28	-1.80	-4.23	-3.60	-5.67	-6.15
Median	11.00	9.80	9.20	10.00	9.20	8.70	8.00	7.50	5.60	2.55	-1.00	-2.00	-3.00	-3.35	-3.40	-6.00	-6.15
Maximum	16.00	15.40	17.40	18.60	16.40	15.40	17.40	21.40	23.20	15.30	13.00	13.90	11.30	3.00	3.00	-3.00	-6.00
Std. Dev.	4.89	4.27	4.60	4.37	4.37	4.25	4.52	5.14	5.17	4.77	4.95	6.45	5.53	3.87	3.91	2.52	0.21
Skewness	-1.49	-0.65	-0.90	-0.65	-0.62	-0.04	0.21	0.57	1.16	0.42	0.75	0.76	0.74	0.02	0.21	0.59	
Kurtosis	6.63	3.99	5.84	6.03	3.75	1.74	2.06	3.32	5.67	4.04	3.45	2.75	3.23	2.54	3.20		
74Entry	-9.50	-8.50	-7.50	-6.50	-5.50	-4.50	-3.50	-2.50	-1.50	-0.50	0.50	1.50	2.50	3.50	4.50	5.50	6.50
Count	15.00	16.00	19.00	23.00	25.00	27.00	27.00	28.00	31.00	31.00	31.00	24.00	10.00	8.00	2.00	2.00	2.00
Minimum	-0.40	-4.00	-4.00	2.80	3.50	1.80	-2.70	-9.00	-9.00	-10.00	-10.00	-7.80	-9.00	-8.00	0.00	-4.00	-6.40
Mean	10.31	10.12	11.04	12.17	11.71	10.20	8.86	7.72	5.84	2.98	1.04	-0.39	-2.81	-3.71	1.00	-3.75	-3.70
Median	10.70	11.35	13.00	13.60	12.20	10.40	9.80	7.90	6.00	3.20	0.00	-1.75	-3.35	-2.55	1.00	-3.75	-3.70
Maximum	20.90	18.90	18.00	18.00	17.90	16.60	15.40	15.60	15.30	11.50	19.00	13.30	6.60	0.00	2.00	-3.50	-1.00
Std. Dev.	5.61	6.22	5.73	4.14	3.62	3.99	4.54	4.81	4.59	5.24	5.82	5.40	5.37	3.66	1.41	0.35	3.82
Skewness	-0.07	-0.83	-1.05	-0.87	-0.43	-0.29	-1.10	-1.50	-0.91	-0.50	0.82	0.85	0.58	-0.35			
Kurtosis	3.29	3.60	4.05	3.15	2.82	2.51	4.41	7.40	5.76	3.01	4.91	3.44	2.33	0.83			
74All	-9.50	-8.50	-7.50	-6.50	-5.50	-4.50	-3.50	-2.50	-1.50	-0.50	0.50	1.50	2.50	3.50	4.50	5.50	6.50
Total Count	37.00	42.00	46.00	50.00	55.00	58.00	60.00	67.00	72.00	73.00	73.00	55.00	33.00	20.00	11.00	5.00	4.00
Grand Min	-5.60	-4.00	-5.30	-3.90	-2.60	1.50	-2.70	-9.00	-9.00	-10.00	-10.00	-10.00	-10.00	-10.00	-10.00	-8.00	-6.40
Grand Average	10.06	9.55	10.09	10.90	10.23	9.55	8.76	7.65	6.03	3.17	0.42	-0.89	-2.11	-4.02	-2.76	-4.90	-4.93
Grand Max	20.90	18.90	18.00	18.60	17.90	16.60	17.40	21.40	23.20	15.30	19.00	13.90	11.30	3.00	3.00	-3.00	-1.00

Table 3b. Same as Table 1 except the data are radar reflectivity for WSR-74C.

88Exit	-9.50	-8.50	-7.50	-6.50	-5.50	-4.50	-3.50	-2.50	-1.50	-0.50	0.50	1.50	2.50	3.50	4.50	5.50	6.50
Count	8	8	9	10	10	10	13	14	15	15	15	9	2	1	1	0	1
Minimum	2.6	4.0	2.6	1.6	-2.0	-0.8	0.0	-1.9	-1.6	-4.4	-8.0	-9.0	-8.0	-4.0	0.6		3.3
Mean	14.3	14.2	15.1	14.8	14.0	14.0	12.0	10.5	10.3	7.8	3.7	1.1	-4.0	-4.0	0.6		3.3
Median	17.0	16.5	18.2	18.3	16.8	16.4	12.2	11.5	11.0	9.8	5.0	1.0	-4.0	-4.0	0.6		3.3
Maximum	21.6	21.6	21.7	20.6	21.6	21.9	21.8	22.0	22.5	20.6	14.4	10.0	0.0	-4.0	0.6		3.3
Std. Dev.	6.4	6.8	7.2	7.1	7.9	7.7	7.1	8.0	8.0	7.7	7.6	6.7	5.7				
Skewness	-0.9	-0.7	-1.1	-1.1	-1.1	-0.9	-0.1	-0.1	-0.2	-0.3	-0.3	-0.1					
Kurtosis	3.0	1.8	2.7	2.7	3.3	2.7	1.7	1.5	1.5	2.1	1.6	1.5					
88Entry	-9.50	-8.50	-7.50	-6.50	-5.50	-4.50	-3.50	-2.50	-1.50	-0.50	0.50	1.50	2.50	3.50	4.50	5.50	6.50
Count	7	7	7	11	12	14	14	14	12	14	14	5	4	2			
Minimum	6.0	6.0	-1.1	-2.3	-2.5	-2.0	0.8	-1.0	3.1	-3.8	-6.0	-4.9	-10.0	-3.0			
Mean	16.5	16.8	15.9	14.7	14.1	11.9	11.8	10.2	9.8	5.5	3.8	3.5	-3.0	-2.0			
Median	19.7	19.2	18.2	16.3	15.5	13.3	13.5	10.1	9.7	6.6	5.5	4.0	-2.9	-2.0			
Maximum	22.2	22.0	21.8	22.0	21.4	20.0	19.9	20.0	18.0	17.4	15.0	14.0	4.0	-1.0			
Std. Dev.	6.0	5.8	7.8	7.2	6.6	6.7	6.3	6.4	5.3	6.4	6.4	6.9	5.8	1.4			
Skewness	-1.0	-1.2	-2.2	-1.5	-1.5	-0.7	-0.4	0.0	0.3	0.0	-0.1	0.7	0.0				
Kurtosis	2.8	3.8	8.3	5.1	5.9	2.6	2.0	2.2	1.7	2.4	2.2	4.4	3.5				
88All	-9.50	-8.50	-7.50	-6.50	-5.50	-4.50	-3.50	-2.50	-1.50	-0.50	0.50	1.50	2.50	3.50	4.50	5.50	6.50
Total Count	15	15	16	21	22	24	27	28	27	29	29	14	6	3	1	0	1
Grand Min	2.60	4.00	-1.10	-2.30	-2.50	-2.00	0.00	-1.90	-1.60	-4.40	-8.00	-9.00	-10.00	-4.00	0.60		3.30
Grand Average	15.30	15.37	15.42	14.75	14.04	12.73	11.86	10.32	10.06	6.71	3.75	1.97	-3.30	-2.67	0.60		3.30
Grand Max	22.20	22.00	21.80	22.00	21.60	21.90	21.80	22.00	22.50	20.60	15.00	14.00	4.00	-1.00	0.60		3.30

Table 4a. Same as Table 2 except the data are radar reflectivity for WSR-88D.

74Exit	-9.50	-8.50	-7.50	-6.50	-5.50	-4.50	-3.50	-2.50	-1.50	-0.50	0.50	1.50	2.50	3.50	4.50	5.50	6.50
Count	5	5	6	7	8	8	11	11	13	14	14	6	2	0	1	2	1
Minimum	-5.50	-8.50	-4.60	-5.00	-4.20	-3.70	-10.00	-9.20	-7.10	-6.80	-7.00	-10.00	-9.10		-6.30	-10.00	-10.00
Mean	8.18	7.44	9.32	8.44	8.24	9.30	7.49	6.80	5.25	0.69	-0.77	-3.63	-5.05		-6.30	-8.00	-10.00
Median	12.90	7.50	12.35	15.30	9.20	11.75	8.80	8.80	6.80	1.60	-2.30	-6.00	-5.05		-6.30	-8.00	-10.00
Maximum	15.00	17.40	17.00	17.50	19.00	18.70	16.20	15.60	17.50	8.40	7.00	4.00	-1.00		-6.30	-6.00	-10.00
Std. Dev.	8.58	10.41	8.59	10.20	9.25	8.58	8.70	8.62	7.51	4.76	4.96	5.80	5.73			2.83	
Skewness	-1.33	-0.91	-0.98	-0.43	-0.21	-0.40	-0.78	-0.81	-0.26	0.05	0.30	0.68					
Kurtosis	3.91	3.49	2.61	0.50	1.02	1.25	2.68	2.55	2.51	2.20	1.42	1.34					
74Entry	-9.50	-8.50	-7.50	-6.50	-5.50	-4.50	-3.50	-2.50	-1.50	-0.50	0.50	1.50	2.50	3.50	4.50	5.50	6.50
Count	3.00	4.00	4.00	6.00	5.00	8.00	6.00	10.00	11.00	11.00	11.00	7.00	4.00	4.00	4.00	2.00	1.00
Minimum	10.10	9.40	2.80	0.90	5.00	1.00	7.60	4.00	-2.00	-6.00	-8.80	-9.00	-9.10	-9.00	-9.00	-3.00	0.60
Mean	12.73	13.30	10.73	11.63	10.60	9.78	13.78	11.15	9.05	4.57	1.48	-0.46	-2.63	-3.33	0.35	0.25	0.60
Median	12.00	13.10	11.45	12.70	9.00	10.25	13.95	9.30	8.00	7.00	-1.20	-3.60	-2.70	-3.80	2.70	0.25	0.60
Maximum	16.10	17.60	17.20	18.00	17.20	15.90	18.20	24.40	25.70	14.90	12.10	7.20	4.00	3.30	5.00	3.50	0.60
Std. Dev.	3.07	4.20	6.47	6.42	5.88	5.42	3.67	7.45	7.96	7.94	7.28	6.44	7.42	6.60	6.43	4.60	
Skewness	1.01	0.08	-0.45	-0.93	0.33	-0.48	-0.81	1.07	0.82	-0.04	0.10	0.10	0.00	0.07	-1.66		
Kurtosis		-2.36	0.83	3.47	-0.02	1.97	4.02	3.06	3.60	1.08	1.28	0.94	-2.98	-2.59	5.71		
74All	-9.50	-8.50	-7.50	-6.50	-5.50	-4.50	-3.50	-2.50	-1.50	-0.50	0.50	1.50	2.50	3.50	4.50	5.50	6.50
Total Count	8	9	10	13	13	16	17	21	24	25	25	13	6	4	5	4	2
Grand Min	-5.50	-8.50	-4.60	-5.00	-4.20	-3.70	-10.00	-9.20	-7.10	-6.80	-8.80	-10.00	-9.10	-9.00	-9.00	-10.00	-10.00
Grand Average	9.89	10.04	9.88	9.92	9.15	9.54	9.71	8.87	6.99	2.40	0.22	-1.92	-3.43	-3.33	-0.98	-3.88	-4.70
Grand Max	16.10	17.60	17.20	18.00	19.00	18.70	18.20	24.40	25.70	14.90	12.10	7.20	4.00	3.30	5.00	3.50	0.60

Table 4b. Same as Table 2 except the data are radar reflectivity for WSR-74C.

REPORT DOCUMENTATION PAGE			Form Approved OMB No. 0704-0188	
<small>Public reporting burden for this collection of information is estimated to average 1 hour per response, including the time for reviewing instructions, searching existing data sources, gathering and maintaining the data needed, and completing and reviewing the collection of information. Send comments regarding this burden estimate or any other aspect of this collection of information, including suggestions for reducing this burden to Washington Headquarters Services, Directorate for Information Operations and Reports, 1215 Jefferson Davis Highway, Suite 1204, Arlington, VA 22202-4302, and to the Office of Management and Budget, Paperwork Reduction Project (0704-0188), Washington, DC 20503.</small>				
1. AGENCY USE ONLY (Leave blank)		2. REPORT DATE 30 September 2004		3. REPORT TYPE AND DATES COVERED Final
4. TITLE AND SUBTITLE Electric Field Magnitude and Radar Reflectivity as a Function of Distance from Cloud Edge			5. FUNDING NUMBERS N/A	
6. Author(s) Jennifer G. Ward and Francis J. Merceret				
7. PERFORMING ORGANIZATION NAME(S) AND ADDRESS(ES) NASA/Kennedy Space Center Kennedy Space Center, FL 32899			8. PERFORMING ORGANIZATION REPORT NUMBER NASA/TM-2004-211530	
9. SPONSORING/MONITORING AGENCY NAME(S) AND ADDRESS(ES) NASA/Kennedy Space Center Kennedy Space Center, FL 32899			10. SPONSORING/MONITORING AGENCY REPORT NUMBER	
11. SUPPLEMENTARY NOTES N/A				
12A. DISTRIBUTION/AVAILABILITY STATEMENT			12B. DISTRIBUTION CODE	
13. ABSTRACT (Maximum 200 Words) <p>The results of analyses of data collected during a field investigation of thunderstorm anvil and debris clouds are reported. Statistics of the magnitude of the electric field are determined as a function of distance from cloud edge. Statistics of radar reflectivity near cloud edge are also determined. Both analyses use <i>in-situ</i> airborne field mill and cloud physics data coupled with ground-based radar measurements obtained in east-central Florida during the summer convective season.</p> <p>Electric fields outside of anvil and debris clouds averaged less than 3 kV/m. The average radar reflectivity at the cloud edge ranged between 0 and 5 dBZ.</p>				
14. SUBJECT TERMS Electric Field Cloud-Physics Meteorology Debris-clouds Anvil-clouds			15. NUMBER OF PAGES 30	
			16. PRICE CODE	
17. SECURITY CLASSIFICATION OF REPORT UNCLASSIFIED		18. SECURITY CLASSIFICATION OF THIS PAGE UNCLASSIFIED		19. SECURITY CLASSIFICATION OF ABSTRACT UNCLASSIFIED
20. LIMITATION OF ABSTRACT UL				
